2D Teager-Kaiser Analysis on Gaussian Noise

EL-Hadji Samba Diop, Abdel-O Boudraa

2D Teager-Kaiser Analysis on Gaussian Noise

1st El Hadji S. Diop
NAGIP Group, Department of mathematics, University Iba Der Thiam, Thies, Senegal

2nd Abdel-O. Boudraa
IMPM Data Group, French Naval Academy IRENav Brest, France

3rd Ndéye N. Gueye
NAGIP Group, Department of Mathematics, University Iba Der Thiam, Thies, Senegal

***Abstract*—We provide here some contributions on the analysis of 2D Teager-Kaiser energy operator (TKEO) on Gaussian noise. To do so, we determine the probability density function (pdf) and the statistical distributions of its output. In addition, we show the asymmetry of the pdf and propose to fit it with a shifted log-Laplace distribution. We provide lower and higher statistical moments, and prove the dependence on the covariance matrix of the noise of both the standard deviation, coefficient of variation, skewness and kurtosis. Finally, we show the ability of 2D higher order statistics to detect object contours in highly noisy images and provide illustrations on both synthetic and real images.**

***Index Terms*—Teager-Kaiser operator. Gaussian noise. Statistical moments. Skewness. Kurtosis.**

I. Introduction

Signals can represent any phenomena. In real world applications, the notion of energy is very important in the sense that signals are always transmitted with a finite total energy [1]–[3]. It is then important to know how to calculate or provide a good approximation of this quantity, which should not depend on the representation of the signals. In that context, an energy measure related to the amplitude modulation (AM) and frequency modulation (FM) was introduced [4], [5], and later extended for analyzing oscillatory signals with time-varying amplitude and frequency in speech processing [6]. This energy measure is known as Teager-Kaiser Energy Operator (TKEO). A relationship was established between TKEO and the class of Volterra filters [7]; see [8], [9] for more about these filers. TKEO has found many applications in various domains, for instance in signal and image demodulation, multiresolution detection, texture analysis, image segmentation, time-frequency analysis [10]–[16]. Some interesting extensions have also been proposed by using k^{th} order derivatives of the signal/image [17], [18], the goal being to improve demodulation results. A good review on TKEO can be found in [19].

There exists only some few works on the behavior of 1D TKEO on noise [20]–[23], most of them proposed computations of lower statistical moments under the assumptions of Gaussian noise or uniformly distributed random signal. Very recently, a thorough analysis of the statistical distributions of 1D TKEO on zero-mean white Gaussian noise was proposed [24], statistical moments were also computed. To the best of our knowledge, there is not yet any 2D study on 2D TKEO in the presence of noise of any type. Here, we propose a 2D analysis and prove that the standard deviation, coefficient of variation, skewness and normalized kurtosis of 2D TKEO outputs of the noise all depend on the covariance matrix of the noise. 1D TKEO output approximates a high pass filter weighted by the local mean [7], this explains 2D TKEO capabilities for edge detection in images. In addition to the theoretical framework, we show the capabilities of higher order statistical moments in detecting objects in images, even in very noisy environment.

II. Background on TKEO and extensions

TKEO output on any discrete signal $s[n]$ is defined by:

$$\Psi(s[k]) = (s[k])^2 - s[k-1]s[k+1]. \tag{1}$$

For any differentiable signal $s(t)$, TKEO is defined as:

$$\Psi[s(t)] = [\dot{s}(t)]^2 - s(t)\ddot{s}(t), \tag{2}$$

where $\dot{s}(t)$ and $\ddot{s}(t)$ represent the first and second derivatives in time of $s(t)$, respectively. Many TKEO extensions have been proposed [17], [18], [25].

The 2D extension denoted 2D TKEO has been extended from 1D TKEO as follows: $\Psi[I(x,y)] = \|\nabla I(x,y)\|^2 - I(x,y)\triangle I(x,y)$, where $I(x,y)$ is an image, $\nabla I(x,y)$ the gradient of I, $\|\cdot\|$ the $\mathbb{R}^2$ euclidean norm and $\triangle I(x,y)$ the Laplacian of image I. The discrete formulation is then obtained $\forall\ (k,l) \in \mathbb{N}^2$, as: $\Psi(I[k,l]) = 2(I[k,l])^2 - I[k-1,l]\cdot I[k+1,l] - I[k,l-1]\cdot I[k,l+1]$.

Proposition 2.1: Let $I[k,l]$ be a discrete image. Its 2D TKEO output can be decomposed as follow:

$$\Psi(I[k,l]) = \Psi(I[k,\cdot]) + \Psi(I[\cdot,l]), \tag{3}$$

where $\Psi(I[k,\cdot])$ and $\Psi(I[\cdot,l])$ are 1D TKEO discrete outputs obtained along lines and columns, respectively.

Proof The proof is straightforward by applying the definition of 2D discrete TKEO and considering for example $\Psi(I[k,\cdot]) = (I[k,l])^2 - I[k-1,l]I[k+1,l]$. ∎

III. TKEO analysis on 2D Gaussian noise

Let $W(t_1,t_2)$ be a Gaussian noise defined on $\mathbb{R}^2$ such that given fixed t_2, $W(\cdot,t_2) \sim \mathcal{N}(0,\sigma_1)$ and given fixed t_1, $W(t_1,\cdot) \sim \mathcal{N}(0,\sigma_2)$. Let $W_1 : t_1 \longmapsto W(t_1,t_2)$ and $W_2 : t_2 \longmapsto W(t_1,t_2)$. W_1 and W_2 are continuous zero-mean random variables with respective standard deviation equals to σ_1 and σ_2. Since axes (O,t_1) and (O,t_2) are independent, then, W_1 and W_2 are also mutually independent. Excitation $W_i(t)$, $i = 1,2$, of TKEO are given by: $\Psi(W_1) = (W_1[k])^2 - W_1[k-1]W_1[k+1]$ and $\Psi(W_2) =$

$(W_2[l])^2 - W_2[l-1]W_2[l+1]$. Then, thanks to Proposition 2.1, the excitation $W(t_1, t_2)$ of 2D TKEO writes:

$$\Psi(W[k,l]) = \Psi(W_1[k]) + \Psi(W_2[l]). \tag{4}$$

We assume excitation $W_1(t)$ and $W_2(t)$ of 1D TKEO is repeated a large number of times, and derived samples are observed values of corresponding random values. TKEO outputs are thus considered as operations on those random values.

Denote $f_{\Psi(W)}$ the pdf of $\Psi(W)$. It provides a good characterization of $\Psi(W)$, the next result provides its form:

Proposition 3.1: The pdf $f_{\Psi(W)}$ of $\Psi(W)$ is given by:

$$f_{\Psi(W)}(t_1,t_2) = \frac{1}{2(\sigma_1\sigma_2\pi)^3}\int_0^\infty\int_0^\infty \frac{1}{\sqrt{x}}\exp\left(-\frac{x^2}{2\sigma_1^2}\right)\times \left(\int_0^\infty \exp\left(-\frac{|t_1-y-x|}{\sigma_1^2}\cosh(u)\right)\mathrm{d}u\right)\mathrm{d}x \int_0^\infty \frac{1}{\sqrt{x}}\exp\left(-\frac{x^2}{2\sigma_2^2}\right) \times \left(\int_0^\infty \exp\left(-\frac{|t_2-y-x|}{\sigma_2^2}\cosh(u)\right)\mathrm{d}u\right)\mathrm{d}x\mathrm{d}y. \tag{5}$$

Proof Since $\Psi(W)$ is the sum of the TKEOs of W_1 and W_2 relatively to their respective standard deviations σ_1 and σ_2, then, its pdf is the convolution of the pdf $f_{\Psi(W_1)}$ of $\Psi(W_1)$ and the pdf $f_{\Psi(W_2)}$ of $\Psi(W_2)$. Then, extending results from [24], [26], one has:

$$f_{\Psi(W)}(t_1,t_2) = \left[f_{\Psi(W_1)}(t_1) * f_{\Psi(W_2)}(t_2)\right] \tag{6}$$

$$= \left[f_{\Psi_{\sigma_1}}(B_1(t_1)) * f_{\Psi_{\sigma_2}}(B_2(t_2))\right] \tag{7}$$

$$= \left[\lambda_{11}\int_0^\infty \frac{1}{\sqrt{x}}\exp\left(-\frac{x^2}{2\sigma_1^2}\right)\left(\int_0^\infty \exp(-\lambda_{12})\,\mathrm{d}u\right)\mathrm{d}x\right] * \left[\lambda_{21}\int_0^\infty \frac{1}{\sqrt{x}}\exp\left(-\frac{x^2}{2\sigma_2^2}\right)\left(\int_0^\infty \exp(-\lambda_{22})\,\mathrm{d}u\right)\mathrm{d}x\right], \tag{8}$$

where $\lambda_{11} = \frac{1}{\sigma_1^3\sqrt{2\pi^3}}$, $\lambda_{21} = \frac{1}{\sigma_2^3\sqrt{2\pi^3}}$, $\lambda_{12} = \frac{|t_1-x|}{\sigma_1^2}\cosh(u)$ and $\lambda_{22} = \frac{|t_2-x|}{\sigma_2^2}\times\cosh(u)$. It follows:

$$f_{\Psi(W)}(t_1,t_2) = \beta\int_0^\infty\left[\int_0^\infty \frac{1}{\sqrt{x}}\exp\left(-\frac{x^2}{2\sigma_1^2}\right)\left(\int_0^\infty \exp(-\lambda_1)\mathrm{d}u\right)\right. \times \left.\left[\int_0^\infty \frac{1}{\sqrt{x}}\exp\left(-\frac{x^2}{2\sigma_2^2}\right)\left(\int_0^\infty \exp(-\lambda_2)\mathrm{d}u\right)\mathrm{d}x\right]\mathrm{d}y, \tag{9}$$

with $\beta = \lambda_{11}\lambda_{21}$, $\lambda_1 = \frac{|t-y-x|}{\sigma_1^2}\cosh(u)$ and $\lambda_2 = \frac{|y-x|}{\sigma_2^2}\cosh(u)$. Let $\lambda = \frac{1}{2\sigma_1^3\sigma_2^3\pi^3}$, thus: $f_{\Psi(W)}(t_1,t_2) = \lambda\int_0^\infty\left[\int_0^\infty \frac{1}{\sqrt{x}}\exp\left(-\frac{x^2}{2\sigma_1^2}\right)\left(\int_0^\infty \exp(-\lambda_1)\mathrm{d}u\right)\mathrm{d}x\right] \times \left[\int_0^\infty \frac{1}{\sqrt{x}}\exp\left(-\frac{x^2}{2\sigma_2^2}\right)\left(\int_0^\infty \exp(-\lambda_2)\mathrm{d}u\right)\mathrm{d}x\right]\mathrm{d}y.$ ∎

Fig. 1 compares the pdfs of $\Psi(b)$ and the zero-mean Gaussian $b(t_1,t_2) \sim \mathbb{N}(\mu,\Sigma)$, with $\mu = (0,0)$ and both with $\sigma_1 = \sigma_2 = 1$. Notice the difference between the pdf of the 2D TKEO output (orange curve) and the Gaussian distribution (in blue). Also, the tail of the skewness of the pdf $f_{\Psi(b)}(t_1,t_2)$ of $\Psi(b)$ gets heavier as the variance of the noise increases (Fig. 1, down). Fig. 2 shows for $\mu = (0,0)$ and $\sigma_1 = \sigma_2 = 1$ the fitting of $f_{\Psi(b)}$ (in orange) with a log-Laplace (LL) distribution with parameters $\delta = 6.32$, $\alpha = -22$ and $\beta = 24.6$ (blue).

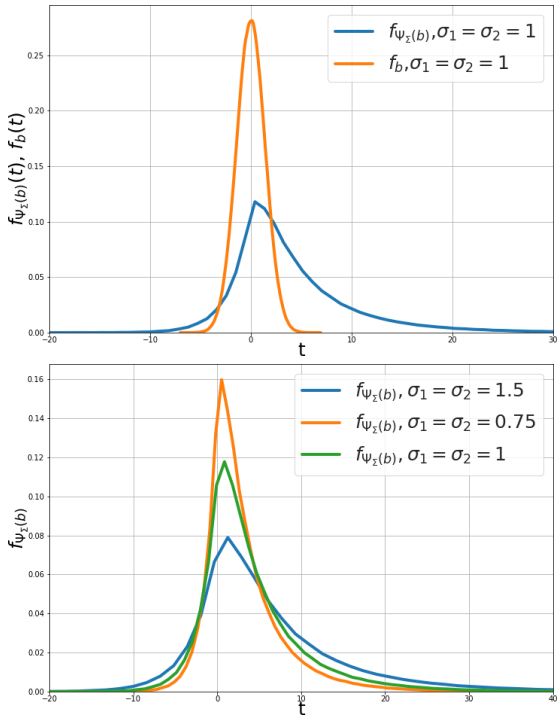

Fig. 1. Probability density function $f_{\Psi(b)}(t_1,t_2)$ of $\Psi(b)$. Top: $b(t_1,t_2) \sim \mathcal{N}((0,0),\Sigma)$. Down: with different values of Σ.

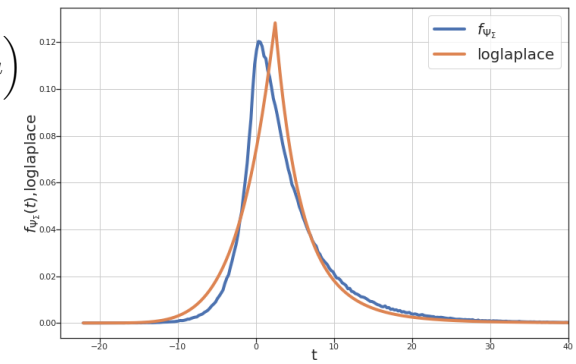

Fig. 2. Approximation of $f_{\Psi(b)}(t_1,t_2)$ by a log-Laplace distribution.

Proposition 3.2: Let W be a WGN with a null mean $(\mu_1,\mu_2) = (0,0)$ and covariance matrix given as: $\Sigma = \begin{pmatrix}\sigma_1 & 0\\ 0 & \sigma_2\end{pmatrix}$. The Expectation, standard deviation and coefficient of variation (CV) of its 2D TKEO output denoted

$\Psi(W)$ are respectively given as:

$$\mathbb{E}(\Psi(W)) = \sigma_1^2 + \sigma_2^2, \tag{10}$$

$$\sigma(\Psi(W) = \sqrt{3}\sqrt{\sigma_1^4 + \sigma_2^4} \text{ and} \tag{11}$$

$$CV(\Psi(W) = \sqrt{3}\frac{\sqrt{\sigma_1^4 + \sigma_2^4}}{\sigma_1^2 + \sigma_2^2}. \tag{12}$$

Proof One has:

• For the expectation. Thanks to decomposition (4) and the independance of variables W_1 and W_2, one has:

$$\mathbb{E}(\Psi(W)) = \mathbb{E}(\Psi(W_1)) + \mathbb{E}(\Psi(W_2)).$$

Use $\mathbb{E}(\Psi(W_i)) = \sigma_i^2$, $i = 1, 2$ [24] to conclude.

• For the standard deviation. Since W_i, $i = 1, 2$, are independent, then, so are their TKEOs. $\mathbb{V}\text{ar}(\Psi(W_i)) = 3\sigma_i^4$, $i = 1, 2$ [24], the decomposition result (4) yields then:

$$\mathbb{V}\text{ar}(\Psi(W)) = \mathbb{V}\text{ar}(\Psi(W_1)) + \mathbb{V}\text{ar}(\Psi(W_2)) = 3\sigma_1^4 + 3\sigma_2^4.$$

• CV definition and equations (10) and (11) yield:

$$\text{CV }(\Psi(W)) = \frac{\sigma(\Psi(W)}{\mathbb{E}(\Psi(W))} = \frac{\sqrt{3(\sigma_1^4 + \sigma_2^4)}}{\sigma_1^2 + \sigma_2^2}. \quad \blacksquare \tag{13}$$

Proposition 3.3: Let W a WGN with a null mean $(\mu_1, \mu_2) = (0, 0)$ and covariance matrix given as: $\Sigma = \begin{pmatrix} \sigma_1 & 0 \\ 0 & \sigma_2 \end{pmatrix}$. The skewness $\gamma(\Psi(W))$ and normalized kurtosis $\kappa(\Psi(W))$ of its 2D TKEO output $\Psi(W)$ are respectively given as follows:

$$\gamma(\Psi(W)) = \frac{8}{3\sqrt{3}} \frac{\sigma_1^6 + \sigma_2^6}{\left(\sqrt{\sigma_1^2 + \sigma_2^2}\right)^3} \text{ and } \kappa(\Psi(W)) = \frac{6(\sigma_1^8 + \sigma_2^8)}{(\sigma_1^4 + \sigma_2^4)^2}. \tag{14}$$

Proof One has:

• Skewness definition and $(W_i)_{i=1}^2$ independence give:

$$\begin{aligned}
\gamma(\Psi(W)) &= \left(\frac{\mathbb{E}(\Psi(W) - \mathbb{E}(\Psi(W))}{\sigma(\Psi(W)}\right)^3 \\
&= \frac{(\mathbb{E}(\Psi(W_1) - \mathbb{E}(\Psi(W_1)) + \Psi(W_2) - \mathbb{E}(\Psi(W_2)))^3}{\sigma^3(\Psi(W))} \\
&= \frac{\mathbb{E}(\Psi(W_1) - \mathbb{E}(\Psi(W_1)))^3 + \mathbb{E}(\Psi(W_2) - \mathbb{E}(\Psi(W_2)))^3}{\sigma(\Psi(W))^3}.
\end{aligned}$$

Since $\sigma(\Psi(W)) = \sqrt{3}\sqrt{\sigma_1^4 + \sigma_2^4}$ and for $i = \{1, 2\}$, $\mathbb{E}(\Psi(W_i) - \mathbb{E}(\Psi(W_i)))^3 = 8\sigma_i^6$, the result follows.

• Kurtosis definition and $(W_i)_{i=1}^2$ independence yield:

$$\begin{aligned}
\kappa(\Psi(W)) &= \left(\frac{\mathbb{E}(\Psi(W) - \mathbb{E}(\Psi(W))}{\sigma(\Psi(W))}\right)^4 - 3 \\
&= \frac{\mathbb{E}(\Psi(W_1) - \mathbb{E}(\Psi(W_1)))^4 + \mathbb{E}(\Psi(W_2) - \mathbb{E}(\Psi(W_2)))^4}{\sigma^4(\Psi(W))} \\
&+ \frac{6\mathbb{E}(\Psi(W_1) - \mathbb{E}(\Psi(W_1)))^2\mathbb{E}(\Psi(W_2) - \mathbb{E}(\Psi(W_2)))^2}{\sigma^4(\Psi(W))} - 3 \\
&= \frac{9((\sqrt{3}\sigma_1^2)^4 + (\sqrt{3}\sigma_2^2)^4) + 6(\sqrt{3}\sigma_1^2)^2(\sqrt{3}\sigma_2^2)^2}{(\sigma_{\Psi(W_1)}^2 + \sigma_{\Psi(W_2)}^2)^2} \\
&- \frac{3((\sqrt{3}\sigma_1^2)^4 + (\sqrt{3}\sigma_2^2)^4 + 2(\sqrt{3}\sigma_1^2)^2(\sqrt{3}\sigma_2^2)^2)}{((\sqrt{3}\sigma_1^2)^2 + (\sqrt{3}\sigma_2^2)^2)^2} \\
&= \frac{6(\sigma_1^8 + \sigma_2^8)}{(\sigma_1^4 + \sigma_2^4)^2}. \quad \blacksquare
\end{aligned}$$

Proposition 3.4: Let $W(t_1, t_2, \cdots, t_n)$ be an nD WGN with expectation $\mu = (\mu_1, \mu_2, \cdots, \mu_n) = (0, 0, ..., 0, 0)$ and a covariance matrix Σ. The expectation, standard deviation and CV of $\Psi[W(t_1, t_2, \cdots, t_n)]$ given by:

$$\mathbb{E}(\Psi(W)) = \sum_{i=0}^{n} \sigma_i^2, \ \sigma(\Psi(W)) = \sqrt{3}\sqrt{\sum_{i=0}^{n} \sigma_i^4}, \text{ and} \tag{15}$$

$$\text{CV }(\Psi(W)) = \sqrt{3}\frac{\sqrt{\sum_{i=0}^{n} \sigma_i^4}}{\sum_{i=0}^{n} \sigma_i^4}. \tag{16}$$

IV. Numerical experiments

Experiments are conducted on synthetic and real images by analyzing with different signal-to-noise ratios (SNRs) the statiscal moments; for instance, the skewness and normalized kurtosis. SNRs range between -25 dB and 50 dB. We consider the following synthetic AM-FM image defined as follows:

$$\begin{aligned}
f_1(k, l) = \frac{1}{2}\cos\left[\frac{\pi}{3}l^5 + \frac{\pi}{5}k + 2\sin\left(\frac{\pi}{30}l + \sin\left(\frac{26\pi}{50}\right)\right)\right] \\
\left[1 + \frac{1}{2}\cos\left(\frac{\pi}{30}l + \frac{\pi}{50}k\right)^2\right],
\end{aligned} \tag{17}$$

where $(k, l) \in \{1, 2, ..., 200\}^2$, and Simba. Images and corresponding TKEOs are displayed in Fig. 3. In our experiments, an additive WGN is added to the test images in the following:

$$g_1(k, l) = f_1(k, l) + b(k, l), \text{ for } i = 1, 2, \tag{18}$$

where $b(k, l) \sim \mathbb{N}(\mu, \Sigma)$, $\mu = (0, 0)$ and $\Sigma = \begin{pmatrix} \sigma_1 & 0 \\ 0 & \sigma_2 \end{pmatrix}$. The values of the skewness and normalized kurtosis of I, Simba and their corresponding 2D TKEO outputs are given in Table I. We display in Fig. 4 the noisy synthetic image g_1 and its corresponding 2D TKEO outputs, g_1 is corrupted with WGNs of SNRs range between -20 dB and 30 dB. We notice a detection of image structures by 2D TKEO up to SNR = -5 dB (Fig. 4), while this cannot be said for the corresponding noisy image at the same SNR rate. This result can also be seen by observing the skewness and normalized kurtosis displayed in Fig. 5 where we notice a slight variation of the skewness of the 2D TKEO $\Psi(g_1)$ output compared to the almost constant

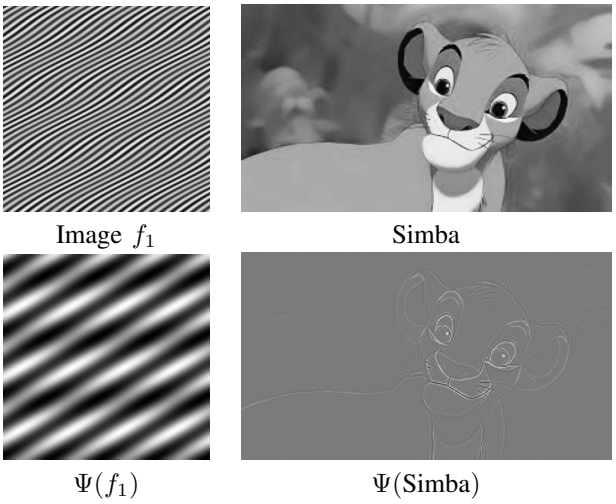

Fig. 3. Synthetic and real images with their corresponding 2D TKEO.

TABLE I
SKEWNESS AND KURTOSIS OF I, SIMBA AND THEIR 2D TKEO.

Images	Skewness (γ)	(κ)
I Eq. (17)	-1.4	-1.4
$\Psi(I)$	0.3	-1.1
Simba	-0.08	0.04
Ψ(Simba)	66.5	3.7

behavior of the skewness of g_1. On the other hand, we notice a variation of the normalized kurtosis for both g_1 and $\Psi(g_1)$ which can be interpreted as the contours detection bounds. Based on the results, we can say that contours of objects can be detected in noisy images for 2D TKEO for the normalized kurtosis values corresponding to SNRs ≥ -10 dB.

Results are also confirmed for Simba, images in Fig. 6 represent the degradations of Simba and their corresponding 2D TKEO outputs, with SNRs range between -10 dB and 40 dB (images below 0 db are not displayed here due to space limitation). We observe a detection of image contours at 0 dB (Fig. 4), this is confirmed by obtained results on the skewness

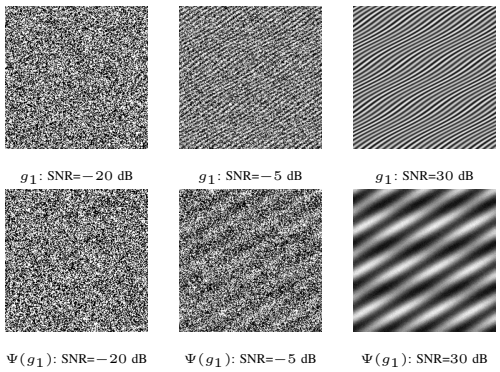

Fig. 4. Displayings with SNRs in between -20 dB and 30 dB. Top line: Noisy image g_1. Bottom: corresponding 2D TKEO $\Psi(g_1)$.

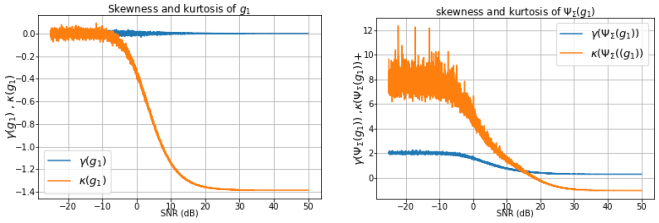

Fig. 5. Kurtosis and skewness with different SNRs. Left: g_1. Right: $\Psi(g_1)$.

and normalized kurtosis displayed in Fig. 7. The variations of the normalized kurtosis in Simba and Ψ(Simba) determine the contours detection bounds. Thus, we can say that the contours of objects can be detected in noisy images for 2D TKEO for non negative normalized kurtosis values corresponding to SNRs ≥ 0 dB.

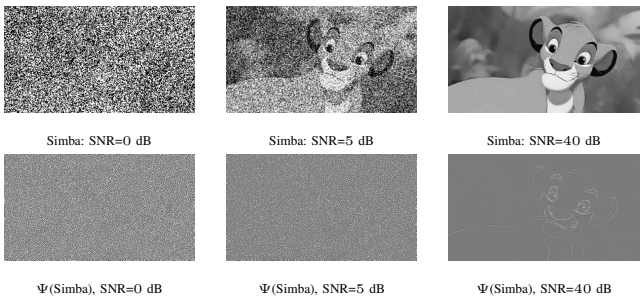

Fig. 6. Displayings with SNRs in between 0 dB and 40 dB. Top line: Simba. Bottom: Corresponding 2D TKEO Ψ(Simba).

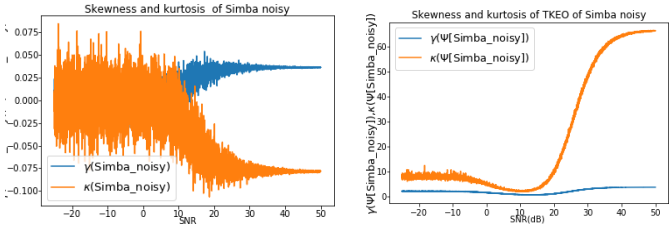

Fig. 7. Kurtosis and skewness with different SNRs. Left: Simba. Right: Ψ(Simba).

V. CONCLUSION

We have proposed here a mathematical analysis of the output of 2D TKEO in a Gaussian noisy environment. To achieve this, we have determined the 2D pdf and the statistical distributions of 2D TKEO outputs. We also have shown the asymmetry of the pdf, and proposed its fitting with a shifted log-Laplace distribution. In addition, we have provided explicit calculations of the standard deviation, coefficient of variation, skewness and normalized kurtosis of 2D TKEO outputs, and shown that all these parameters depend on the covariance matrix of the noise. Besides the theoretical contributions, we have shown the capabilities of the higher order statistics for objects detection in highly noisy images. Ongoing works are on its applications for image enhancement. We plan as well to study TKEO extensions on different types of noise, and under the assumption of dependence of the variables.

REFERENCES

[1] L. Cohen, *Time-Frequency Analysis*. NJ: Prentice Hall, Englewood Cliffs, 1995.

[2] B. Boashash, *Time Frequency Signal Analysis and Processing: A Comprehensive Reference*. The Boulevard, Langford Lane, Kidlington, Oxford OX5 1GB, UK: Elsevier, 2003.

[3] S. Mallat, *A Wavelet Tour of Signal Processing*, A. Press, Ed. Elsevier Science Publishing Co Inc, Dec. 2008.

[4] H. M. Teager, "Some Observations on Oral Air Flow During Phonation," *IEEE ASSP*, vol. ASSP-28, no. 5, pp. 599–601, Oct. 1980.

[5] H. M. Teager and S. M. Teager, "Evidence for nonlinear sound production mechanisms in the vocal tract," in *Speech Production and Speech Modelling*. Springer Netherlands, 1990, pp. 241–261.

[6] J. F. Kaiser, "On a simple algorithm to calculate the 'energy' of a signal," in *IEEE ICASSP*, Apr. 1990, pp. 381–384.

[7] M. Moore, S. Mitra, and R. Bersntein, "A generalization of the Teager algorithm," in *IEEE Worksop NSP*, 1997, pp. 1–4.

[8] F. Kuech and W. Kellermann, "Partitioned block frequency-domain adaptive second-order volterra filter," *IEEE Transactions on Signal Processing*, vol. 53, no. 2, pp. 564–575, feb 2005.

[9] T. Burton, R. Goubran, and F. Beaucoup, "Nonlinear system identification using a subband adaptive volterra filter," *IEEE Transactions on Instrumentation and Measurement*, vol. 58, no. 5, pp. 1389–1397, may 2009.

[10] P. Maragos, "Slope Transforms: Theory and Application to Nonlinear Signal Processing," *IEEE Transactions on Signal Processing*, vol. 43, no. 4, pp. 864–877, 1995.

[11] J. Choi and T. Kim, "Neural action potential detector using multiresolution TEO," *Electronics Letters*, vol. 38, no. 12, p. 541, 2002.

[12] I. Kokkinos, G. Evangelopoulos, and P. Maragos, "Texture analysis and segmentation using modulation features, generative models, and weighted curve evolution," *IEEE Transactions on Pattern Analysis and Machine Intelligence*, vol. 31, no. 1, pp. 142–157, jan 2009.

[13] E. H. S. Diop, A. O. Boudraa, and F. Salzenstein, "A joint 2D AM–FM estimation based on higher order Teager–Kaiser energy operators," *Signal, Image and Video Processing*, vol. 5, no. 1, pp. 61–68, Mar. 2011.

[14] J. Cexus and A. Boudraa, "Nonstationary signals analysis by teager-huang transform (tht)," in *EUSIPCO*, Florence, Italy, 2006.

[15] A. Bouchikhi, A.-O. Boudraa, J.-C. Cexus, and T. Chonavel, "Analysis of multicomponent LFM signals by teager huang-hough transform," *IEEE Transactions on Aerospace and Electronic Systems*, vol. 50, no. 2, pp. 1222–1233, apr 2014.

[16] F. Salzenstein and A.-O. Boudraa, "Multidimensional directional derivatives and AM-FM dual-band image demodulation by higher order teager-kaiser operators," *Digital Signal Processing*, vol. 129, p. 103641, sep 2022.

[17] P. Maragos and A. Potamianos, "Higher order differential energy operators," *IEEE Signal Processing Letters*, vol. 2, no. 8, pp. 152–154, August 1995.

[18] F. Salzenstein, A. Boudraa, and J. Cexus, "Generalized higher-order nonlinear energy operators," *J. Opt. Soc. Amer. (A).*, vol. 24, no. 12, pp. 3717–3727, 2007.

[19] A.-O. Boudraa and F. Salzenstein, "Teager-kaiser energy methods for signal and image analysis: A review," *Digital Signal Processing*, vol. 78, pp. 338–375, jul 2018.

[20] A. Bovik, P. Maragos, and T. Quatieri, "AM-FM energy detection and separation in noise using multiband energy operators," *IEEE Transactions on Signal Processing*, vol. 41, no. 12, pp. 3245–3265, 1993.

[21] D. Dimitriadis, A. Potamianos, and P. Maragos, "A comparison of the squared energy and teager-kaiser operators for short-term energy estimation in additive noise," *IEEE Transactions on Signal Processing*, vol. 57, no. 7, pp. 2569–2581, jul 2009.

[22] P. K. Banerjee and N. B. Chakrabarti, "Noise sensitivity of teager-kaiser energy operators and their ratios," in *2015 International Conference on Advances in Computing, Communications and Informatics (ICACCI)*. IEEE, aug 2015.

[23] M. Jabloun, P. Ravier, and O. Buttelli, "On the statistical properties of the generalized discrete teager-kaiser energy operator applied to uniformly distributed random signals," in *2018 IEEE Statistical Signal Processing Workshop (SSP)*. IEEE, jun 2018.

[24] Y. Preaux and A.-O. Boudraa, "Statistical behavior of teager-kaiser energy operator in presence of white gaussian noise," *IEEE Signal Processing Letters*, vol. 27, pp. 635–639, 2020.

[25] J. Kaiser, "Some useful properties of teager's energy operators," in *IEEE International Conference on Acoustics Speech and Signal Processing*. IEEE, 1993.

[26] R. E. Gaunt, "Products of normal, beta and gamma random variables: Stein operators and distributional theory," *Brazilian Journal of Probability and Statistics*, vol. 32, no. 2, may 2018.